Electromagnetic modelling of the SKA-LOW AAVS1.5 prototype

David B. Davidson
ICRAR
Curtin University
Perth, WA, Australia
david.davidson@curtin.edu.au

Pietro Bolli
Osservatorio Astrofisico di Arcetri
Istituto Nazionale di Astrofisica, OAA-INAF
Florence, Italy
pbolli@arcetri.inaf.it

Mirko Bercigli
Ingegneria Dei Sistemi S.p.A.
IDS
Pisa, Italy

Paola Di Ninni
Osservatorio Astrofisico di Arcetri
Istituto Nazionale di Astrofisica, OAA-INAF
Florence, Italy
dininni@arcetri.inaf.it

Rowanne Steiner
ICRAR
Curtin University
Perth, WA, Australia
and TU Eindoven, The Netherlands

Steven Tingay
ICRAR
Curtin University
Perth, WA, Australia
s.tingay@curtin.edu.au

Daniel Ung
ICRAR
Curtin University
Perth, WA, Australia
daniel.ung@curtin.edu.au

André van Es
SKA Organization
Jodrell Bank, Cheshire, UK
A.vanEs@skatelescope.org

Giuseppe Virone
IEIIT-CNR Turin, Italy
giuseppe.virone@ieiit.cnr.it

Randall Wayth
ICRAR
Curtin University
Perth, WA, Australia
R.Wayth@curtin.edu.au

***Abstract*—The numerical modelling of the Square Kilometre Array (SKA) Aperture Array Verification System Version 1.5 is discussed. The role of this SKA prototype is placed within the perspective of the overall SKA project. The dual-polarized log-periodic SKALA4.1 antenna elements comprising a station are briefly described, along with some considerations regarding the station. Computational simulation aspects are considered, and preliminary results shown. An appraisal of the implications for station-level calibration concludes the paper.**

***Index Terms*—Antenna arrays, phased arrays, radio astronomy, radio interferometry, Square Kilometre Array radio telescope**

I. Introduction

The Square Kilometre Array (SKA) project is an international effort to build the world's largest radio telescope [1]. The intention is eventually deploy over a square kilometre (one million square metres) of collecting area, over two sites primarily hosted in Australia and South Africa. With the pre-construction consortia closing out their activities in a series of Critical Design Reviews in the 2018–19 timeframe, and with the signing of the international treaty establishing the intergovernmental SKA Observatory (SKAO) on 12th March 2019, work is now progressing on a bridging project phase before construction plans are finalised.

Work in Australia and Italy focusses on the deployment, simulation, measurement, calibration and commissioning of a new low-frequency aperture array prototype station, with nominal frequency coverage 50–350 MHz. Known as the Aperture Array Verification System Version 1.5 (AAVS1.5), this continues the trajectory of previous deployments on the MRO. (These include AAVS0.5, circa 2014 and AAVS1.0, circa 2016 [2]. Note that not all of the 400 antennas originally planned for AAVS1.0, as indicated in [2], were deployed — eventually, only one station with 256 antennas was constructed). The station presently under construction, and the topic of this paper, uses a prototype implementation of the reference design (a dual-polarised log-periodic antenna) known as the SKALA4.1 [3].

The main aim of this specific prototype is to further investigate issues relating to the calibratability of a station consisting of a large number of these antennas. Presently, each of the 512 SKA-LOW stations is to comprise 256 of SKALA4s, deployed in a semi-random layout with a maximum antenna-boom-to-boom diameter of 38m. (The ground mesh extends out to an approximate diameter of 42m). Due to the short timeframe of this project, 48 SKALA4s have initially been deployed in the first phase of the project, expanding to either 128 or the full 256 in the second phase, presently planned for later in 2019. A key point is to model the embedded element patterns (EEPs) of each antenna [4, Chapter 4], which current work indicates will be needed for station calibration. This paper will provide an update on the status of this, and outline a drone measurement campaign to validate our simulations of these patterns.

II. The AAVS 1.5 prototype

A. The SKALA4.1 antenna

The SKA-Low Antenna element, SKALA, is currently in its fourth major iteration. The system considerations that led

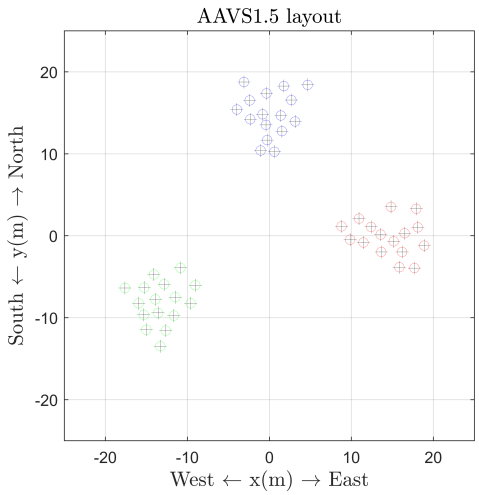

Fig. 1. Layout of the AAVS1.5 array.

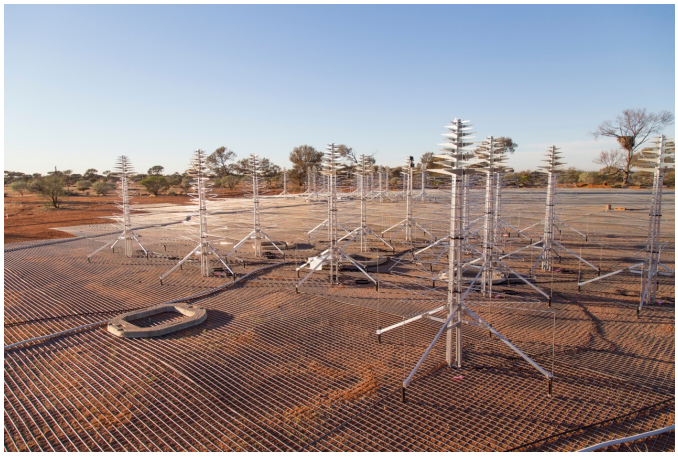

Fig. 2. The AAVS1.5 array on the Murchison Radio-astronomy Observatory, May 2019, showing a close-up view of one of the 16 SKALA4.1 antenna clusters. Credits: ICRAR/Curtin.

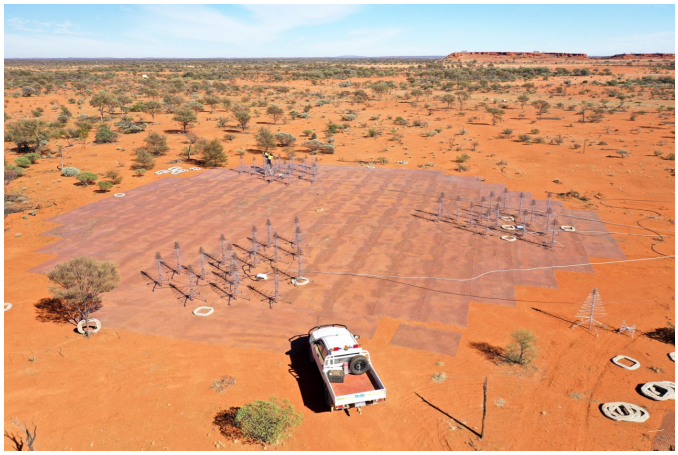

Fig. 3. A "drone's eye" view of the AAVS1.5 array under construction, May 2019. Credits: ICRAR/Curtin.

to the adoption of a (dual) log-periodic design are presented in [5], which also describes the first and second versions of the design, and the current reference design is documented in [3]. The AAVS1.5 station currently comprises 48 SKALA4.1 antennas, built by Italian company Sirio Antenne. Key points of this design are a 50 Ω input impedance, aluminum alloy material construction, and antenna grounding. Further details of the SKALA4.1 may be found in [6].

B. Station layout

Construction of this latest prototype is taking place under the auspices of the SKAO's "bridging" tasks. Designed to address issues flowing from the pre-construction period, these tasks emphasise rapid deployment and testing, and have aggressive time-schedules. The first 48 antennas have been deployed in three clusters of 16, arranged approximately in a triangle inscribed within the station. This arrangement was chosen to provide sufficiently long base-lines to permit the use of the sun for calibration, and is shown in Fig. 1. Deployment was completed shortly before writing. A picture of two of the three clusters is shown in Fig. 2; Fig. 3 provides an overall perspective of the station, taken from a UAV.

III. Numerical Modelling of the AAVS Array

A. Modelling the SKALA4.1 antenna

The SKALA4.1 is appreciably more complex to model numerically than its predecessor in the AAVS1.0, the SKALA2, not least in terms of the use of solid metal elements at the high-frequency end. FEKO [7] and Galileo models have been developed that retain sufficient fidelity to accurately predict input impedance across the frequency range of interest, whilst simplifying some of the geometrical features of the as-built structure. Examples of such simplifications included some approximations for the boom model, removing small plate structures towards the top of the antenna, and removing other small details (e.g. an access hole) which did not provide electromagnetic functionality. This model required just under 12 000 unknowns — by comparison, an initial model derived from CAD files required over 29 000 unknowns. Reflection coefficient results for the simplified model, compared to measured data, are shown in Fig. 4; very good agreement is noted.

B. Array simulations

Full simulations of 48 SKALA4.1 elements exceed the capacity of the standard method of moments (MoM) solvers, and the multi-level fast mutipole algorithm (MLFMA) has been used to compute embedded element patterns. (An overview of this algorithm may be found in [8].) FEKO simulations have been carried out on a recently-acquired DEC PowerEdge 740 server, currently dedicated to this work. This system has dual Xeon Platinum 8180 processors with a total of 56 cores, and has 1.5 TB of RAM available.

Modelling has also been undertaken using the commercial software Galileo-ElectroMagnetic Toolkit, which also offers MLFMA acceleration. More details on this are available in [6]. Other methods have also been proposed and applied, although these are not yet available in commercial solvers [9].

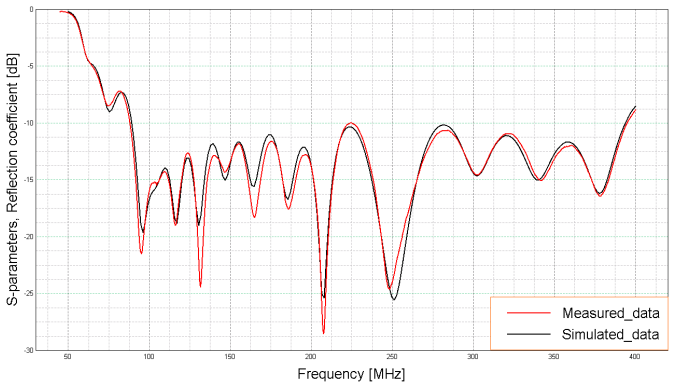

Fig. 4. A comparison of a simplified FEKO model of the SKALA4.1 antenna (black) with measurements (red).

IV. Preliminary results

A comparison of the results obtained for one EEP is shown in Fig. 5. All the EEPs in this work have been computed for a matched 50 Ω load at all ports, other than the port under test. The results show excellent agreement; as noted, both codes use the MoM and make similar assumptions regarding an infinite PEC ground plane, approximating the actual finite wire mesh ground plane. With the full set of embedded element patterns and the array mutual coupling matrix (which can be computed at the same time) the radiation pattern of the array — station beam, in radio astronomy parlance — can be computed. Note that unlike the classical array factor method, which assumes identical element patterns, this approach provides a rigorous solution, fully incorporating mutual coupling. An example for a station beamformed with uniform amplitude and phase weights is shown in Fig. 6 — the beam is directed towards zenith. This figure compares the beams synthesised from the EEPs computed by both the FEKO and Galileo software. Excellent agreement is noted. These patterns have been computed for the transmit case; reciprocity ensures identical patterns for the receive case relevant to a radio telescope. (Note that it is only the antenna and the medium into which it transmits/receives from which need be reciprocal; the radio frequency front-end and other active stages are handled separately [4].)

Simulations involving EEPs generate a large volume of data, since there is an EEP for each antenna. A statistical analysis can be helpful in understanding the overall trends; in Figs. 7, 8 and 9, results for the E-plane gains are shown, computed at 50 MHz. Results are shown for phase in Figs. 10, 11 and 12. These will now be discussed in more detail.

Figs. 7 and 10 shows all 48 EEPs; the inter-element variation is striking. Fig. 8 shows the average EEP, $\underline{\text{EEP}}$[1], compared to the isolated element pattern (IEP); $\underline{\text{EEP}} \pm$ std indicates the one (unnormalized) standard deviation envelope for gain. Fig 11 shows the same results for the phase terms. Figures of merit for the gains are shown in Fig. 9. Here, $\text{std}_{\texttt{norm}}$ is used to indicate the standard deviation normalized (theta by theta) to the average gain, and $\epsilon(\text{IEP},\underline{\text{EEP}})_{\texttt{norm}}$ indicates the absolute difference between $\underline{\text{EEP}}$ and IEP, normalized to the maximum of the average EEP. The corresponding results for phase are shown in Figs. 12; here, $\text{std}_{\texttt{norm}}$ is used to indicate the standard deviation normalized (theta by theta) to the average gain and $|EEP - IEP|_{norm}$ is used to indicate the absolute difference between phase of IEP and phase of EEP, normalized (theta by theta) for the average gain.

By comparison, simulation results are also shown for 320 MHz in Figs. 13–18. Not only is the wavelength shorter, but the active part of the log-periodic antennas is also separated by a larger absolute distance. The result is a much smaller inter-element variability. (It should be noted that most of the key science currently proposed for SKA-LOW prioritises the lower frequency end of the band, where the inter-element variability is large, as shown above.)

[1]Note that $\underline{\text{EEP}}$ (underlined) is the average of the embedded element patterns.

V. Conclusions and next steps

A drone campaign was underway at the time of submission of this paper, with the aim of validating the simulated station results. Due to the remote, radio-quiet location, and sometimes unfavourable weather, this type of measurement requires significant planning and logistical support. Successful results have been obtained on earlier prototype arrays [10], [11].

However, the simulation and measurement of the embedded element patterns is not an end in itself; the key question still to be addressed is whether the significant variation in element patterns, caused by mutual coupling, will permit sufficiently accurate and rapid station-level calibration for SKA-LOW. As demonstrated by these preliminary simulations, the inter-element variability is especially pronounced at the lower end of the frequency band. Existing calibration scheme generally assume that all the EEPs are similar, and the results computed here clearly challenge this assumption.

Acknowledgment

AAVS1.5 is hosted by the MWA under an agreement via the MWA External Instruments Policy. This scientific work makes use of the Murchison Radio-astronomy Observatory, operated by CSIRO. We acknowledge the Wajarri Yamatji people as the traditional owners of the Observatory site.

References

[1] P. E. Dewdney, P. J. Hall, R. T. Schilizzi, and T. J. L. W. Lazio, "The Square Kilometre Array," *Proceedings of the IEEE*, vol. 97, no. 8, pp. 1482–1496, Aug 2009.

[2] P. J. Hall, P. Benthem, and A. T. Sutinjo, "Aperture array verification system 1: Overview of a Square Kilometre Array prototype," in *2016 International Conference on Electromagnetics in Advanced Applications (ICEAA)*, Sep. 2016, pp. 345–348.

[3] E. de Lera Acedo, G. Virone, P. Bolli, H. Pienaar, A. Tibaldi, B. Van Ha, B. Wakley, N. Draught, N. Razavi, and A. Faulkner, "SKA-1-LOW antenna selection — description of the LPD antenna candidates," Aug. 2017, SKAO LFAA Antenna & LNA Work Package, AADC Consortium.

[4] K. F. Warnick, R. Maaskant, M. Ivashina, D. B. Davidson, and B. Jeffs, *Phased Arrays for Radio Astronomy, Remote Sensing, and Satellite Communications*. Cambridge, UK: Cambridge University Press, 2018.

[5] E. de Lera Acedo, N. Razavi-Ghods, N. Troop, N. Drought, and A. J. Faulkner, "SKALA, a log-periodic array antenna for the SKA-low instrument: design, simulations, tests and system considerations," *Experimental Astronomy*, vol. 39, no. 3, pp. 567–594, Oct 2015.
[6] P. Di Ninni, M. Bercigli, P. Bolli, G. Virone, and S. J. Wijnholds, "Mutual coupling analysis for a SKA1-LOW station," in *Proceedings of the 13th European Conference on Antennas and Propagation*, April 2019, pp. 1–5.
[7] "Altair, FEKO, Suite 2018." [Online]. Available: www.feko.info
[8] D. B. Davidson, *Computational Electromagnetics for RF and Microwave Engineering*, 2nd ed. Cambridge, UK: Cambridge University Press, 2011.
[9] H. Bui-Van, J. Abraham, M. Arts, Q. Gueuning, C. Raucy, D. Gonzlez-Ovejero, E. de Lera Acedo, and C. Craeye, "Fast and accurate simulation technique for large irregular arrays," *IEEE Transactions on Antennas and Propagation*, vol. 66, no. 4, pp. 1805–1817, April 2018.
[10] A. T. Sutinjo, T. M. Colegate, R. B. Wayth, P. J. Hall, E. de Lera Acedo, T. Booler, A. J. Faulkner, L. Feng, N. Hurley-Walker, B. Juswardy, S. K. Padhi, N. Razavi-Ghods, M. Sokolowski, S. J. Tingay, and J. G. Bij de Vaate, "Characterization of a low-frequency radio astronomy prototype array in Western Australia," *IEEE Transactions on Antennas and Propagation*, vol. 63, no. 12, pp. 5433–5442, Dec 2015.
[11] E. de Lera Acedo, P. Bolli, F. Paonessa, G. Virone, E. Colin-Beltran, N. Razavi-Ghods, I. Aicardi, A. Lingua, P. Maschio, J. Monari, G. Naldi, M. Piras, and G. Pupillo, "SKA aperture array verification system: electromagnetic modeling and beam pattern measurements using a micro UAV," *Experimental Astronomy*, vol. 45, no. 1, pp. 1–20, Mar 2018. [Online]. Available: https://doi.org/10.1007/s10686-017-9566-x

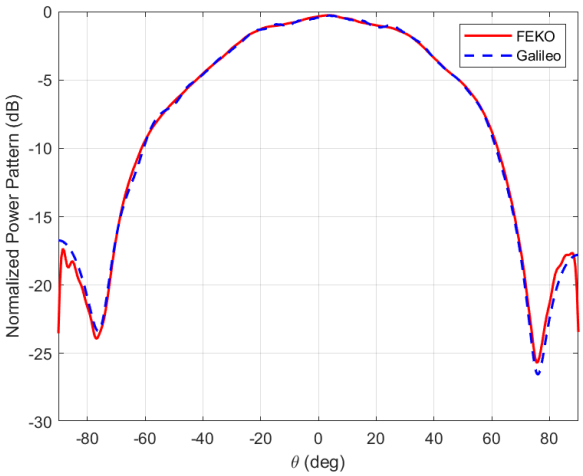

Fig. 5. A comparison of an embedded element pattern computed using the FEKO and Galileo simulation packages. This is for antenna 2, the East–West (X) polarization, at 110 MHz.

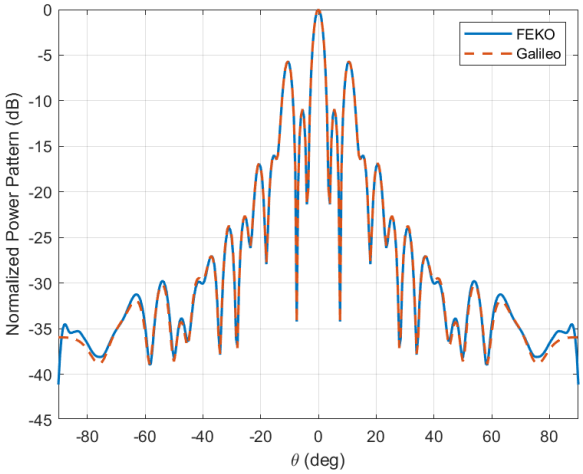

Fig. 6. A comparison of the zenith-pointing station beams, E-plane, synthesized from the EEPs computed using FEKO and Galileo. This is for the East–West (X) polarization, at 110 MHz.

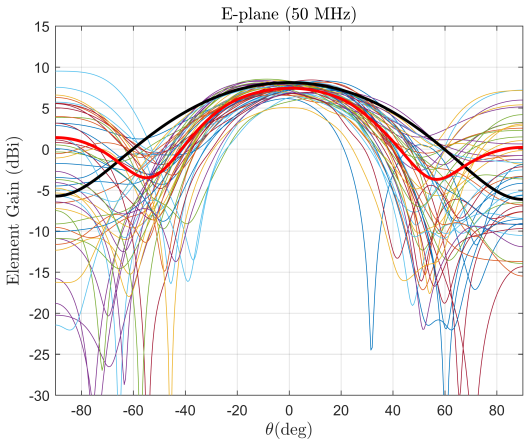

Fig. 7. All EEPs gains, 50 MHz

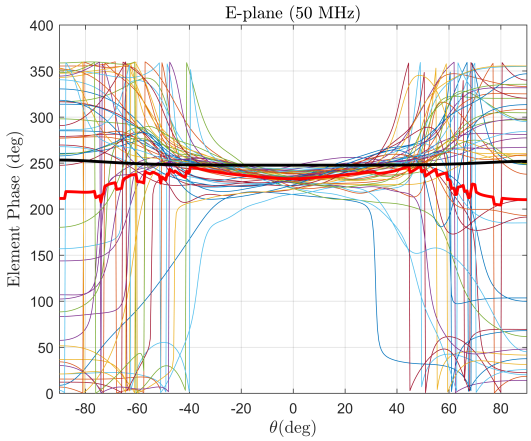

Fig. 10. All EEP phases, 50 MHz

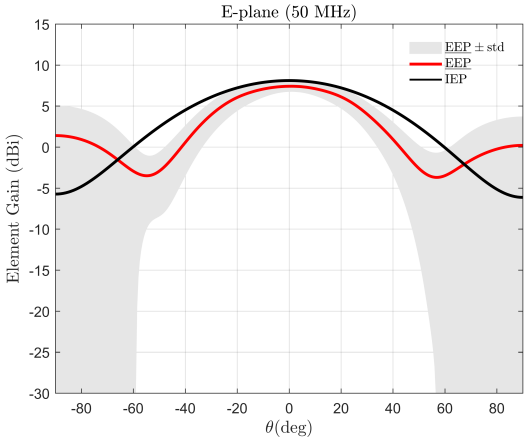

Fig. 8. Average embedded element pattern gain (EEP), compared to isolated element pattern, 50 MHz, also showing 1 σ envelope.

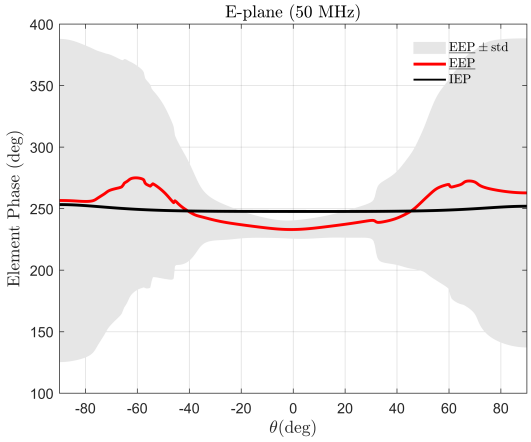

Fig. 11. Average embedded element pattern (EEP) phase, compared to isolated element pattern, 50 MHz, also showing 1 σ envelope.

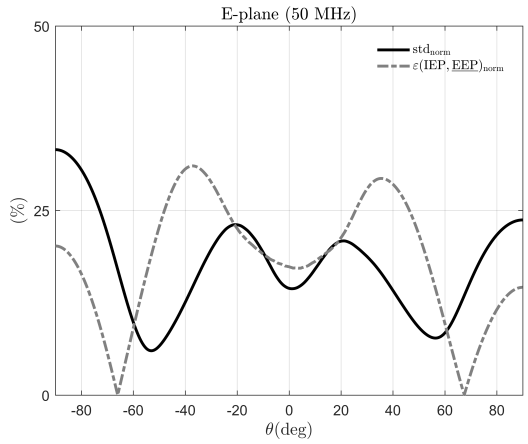

Fig. 9. Figures of merit for the gains, 50 MHz. See text for details.

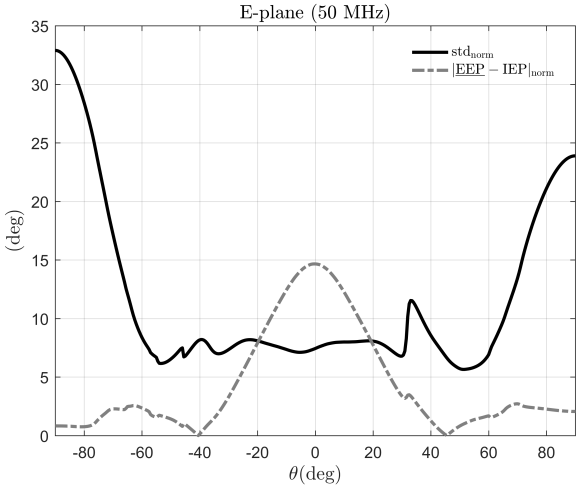

Fig. 12. Figures of merit for the phases, 50 MHz. See text for details.

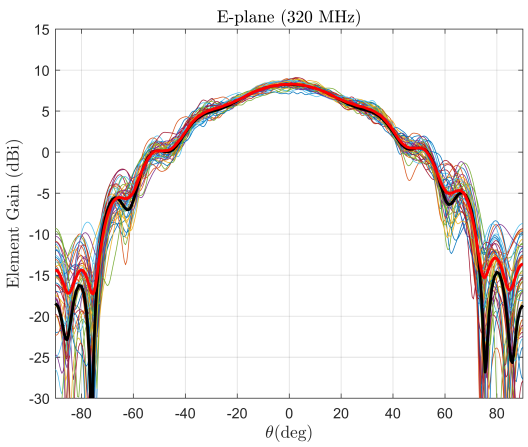

Fig. 13. All EEPs gains, 320 MHz

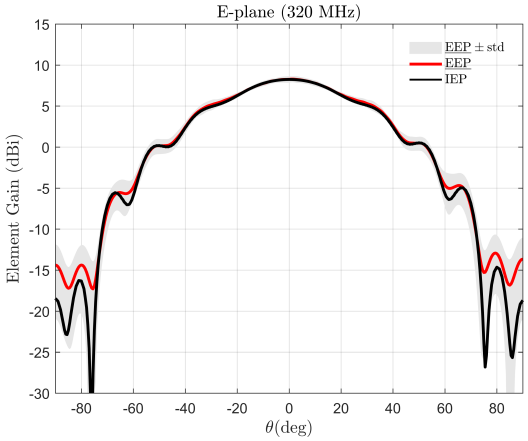

Fig. 14. Average embedded element pattern (EEP) gain, compared to isolated element pattern, 320 MHz, also showing 1 σ envelope.

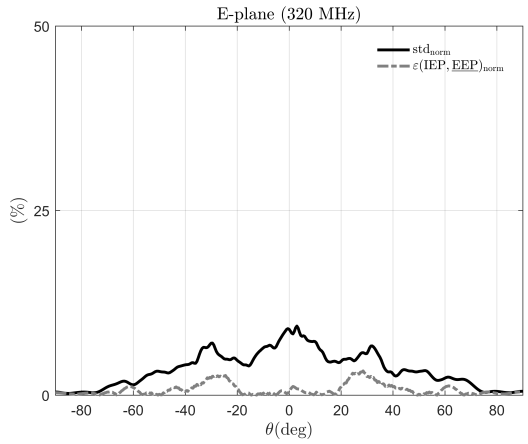

Fig. 15. Figures of merit for the gains, 320 MHz. See text for details.

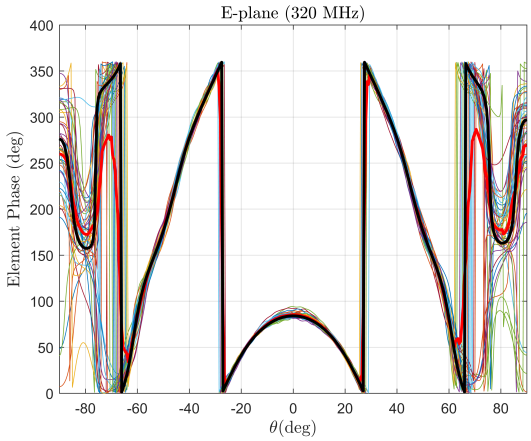

Fig. 16. All EEP phases, 320 MHz

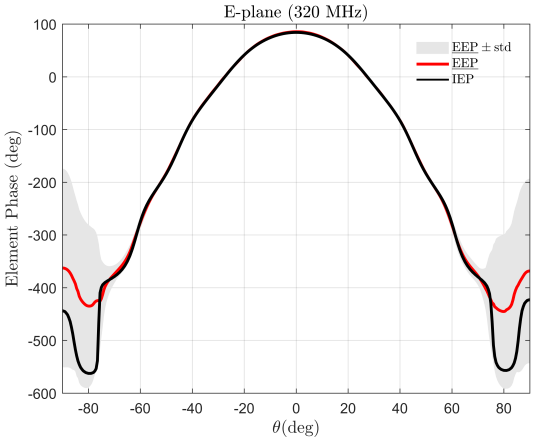

Fig. 17. Average embedded element pattern (EEP) phase, compared to isolated element pattern, 320 MHz, also showing 1 σ envelope.

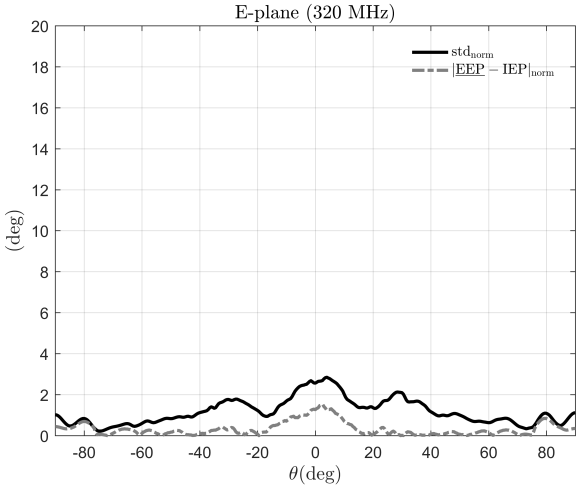

Fig. 18. Figures of merit for the phases, 320 MHz. See text for details.